

# 3D Acoustic-Structure Interaction of Ultrasound in Fluids for the Manufacture of Graded Materials

J. A. Holt\*, C. Torres-Sanchez and P. P. Conway

The Wolfson School of Mechanical, Electrical and Manufacturing Engineering, Loughborough University, Loughborough, LE11 3TU, UK.

j.holt@lboro.ac.uk

\*Corresponding author

**Abstract:** Functionally graded materials engineered to meet specific requirements are being increasingly sought after for advanced engineering projects, yet the possibilities for their manufacture lag behind their design. The ability to control the porosity of a cellular material is one such method for adding functional gradients within materials. A novel technique using ultrasound to control the porosity in reacting polymers shows potential to effectively mass-manufacture porosity tailored polymeric foams. In this work the pressure field in a metastable polymer produced by multiple ultrasonic sources is modeled at distinct stages of the polymerisation reaction.

**Keywords:** ultrasound, functionally graded materials, polymer, foam, sonication

## 1. Introduction

Functionally graded materials (FGM) are those that contain chemical, phase or structural gradients. The result is a non-homogeneous microstructure and position-dependent thermal, mechanical, acoustic or electrical properties [1]. FGMs attempt to address the weaknesses caused by discontinuities in properties within bulk materials by grading these changes and reducing stress concentrations through heterogeneity within the material [2]. The design of such structures can be seen in a range of structural optimisation methods, where one or more design parameters are allowed to vary throughout the structure. Examples are the reinforcing phase of a composite material or the density of a foamed material.

Whilst the design of functionally graded structures is well researched in areas such as shape optimisation and topology optimisation [3]–[5], their manufacture is still in development [6], [7]. One potential method for manufacturing functional gradients within materials is the application of sonication, this is, pressure gradients produced by steady state ultrasonic acoustic fields applied to a metastable material that solidifies [8].

A bubble in a standing-wave acoustic field will experience an oscillating pressure gradient causing the bubble's volume to oscillate. The phase at which the bubble oscillates in relation to the acoustic field is related to the size of the bubble and the frequency of the oscillations. A bubble of less than the resonant size for a particular acoustic frequency will travel up the pressure gradient, whilst a bubble of greater than resonant size will travel down the gradient to the pressure node [9]. Through this mechanism it is possible to influence the distribution of bubbles within a fluid. If that fluid is a metastable polymer undergoing polymerisation, the application of sound can facilitate the control of the macroscopic porous structure.

The manufacture of graded materials using of acoustic fields offers exciting opportunities to produce truly 3-dimensional gradients. Understanding how this manufacturing process works requires an accurate model of fluid-structure interactions between oscillating ultrasonic transducers and an enclosed fluid. In this paper the interaction of a fluid excited by ultrasonic waves in a purpose-built experimental rig is investigated. The work presents a validated 3-dimensional model for oscillating transducers generating a steady-state acoustic field in water. The model is then used to predict the resulting acoustic fields in a polymeric foam for a number of excitation frequencies and transducer configurations.

## 2. Simulation

### Building the Model Geometry

The model geometry (shown in Figure 2, based on the experimental rig shown in Figure 1) was built using the geometry tools available in COMSOL Multiphysics version 5.2a. Each of the transducers was modelled as a single solid cone of aluminium attached to the thin emitting surface which couples the oscillation of the transducer to the fluid. Only the transducer emitting cone was constructed in the

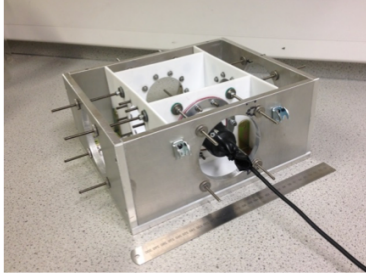


Figure 1. Image of the experimental rig with a single transducer attached. The outer supporting structure is aluminium and the inner vessel walls are PTFE in this image.

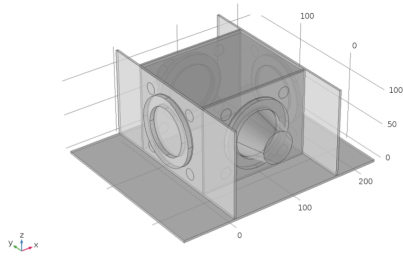


Figure 2. The experimental rig geometry built in COMSOL Multiphysics.

model, the face which makes contact to the piezoelectric element was used to simulate the transducer movement by a prescribed displacement. The external aluminium supporting structure (Figure 1 and Figure 2) was not included and instead it was approximated by a stiff external support modelled at the contact point. The vessel domain (all the rigid structures) was filled with a domain to represent the fluid.

Materials were chosen from the COMSOL Materials Library and applied to the corresponding domain. The walls and the transducers were set to aluminium, the base was set to PTFE, the fluid was set to water and the air domain was set to air.

### Application of Physics

The two physics modules used for this model were the Structural Mechanics Module and the Pressure Acoustics, Frequency Domain Module. Structural Mechanics was used to define the properties of the solid elements. The material model was set to linear elastic and a damping node was applied to this material model taking the isotropic loss factor from the COMSOL Materials Library for each material. All the boundaries were considered free except the bottom of the base plate, to which a zero  $z$ -axis (vertical) displacement constraint was added. To simulate the silicone sealant that makes the vessel watertight a thin elastic layer was applied between the vessel walls with a spring constant of

1E5 N/m. The external supports were modelled using a spring foundation boundary applied to four spherical pads on each vessel wall with a value of 1E12 N/m.

The transducer oscillation was simulated by applying a prescribed displacement to the outermost face of the transducer cone (the face that would contact the piezoelectric element). The maximum displacement amplitude of the transducer,  $D_{Trans}$ , was calculated from:

$$D_{Trans} = \sqrt{\frac{2I}{\rho c_s \omega^2}}$$

where  $\rho$  is the density of the transducer material,  $c_s$  is the speed of sound in the transducer material,  $\omega$  is the angular frequency ( $\omega = 2\pi f$ ) and  $I$  is the acoustic intensity ( $I = P_{Trans}/2\pi r^2$ , where  $P_{Trans}$  is the transducer power and  $r$  is the transducer face radius). For the case of multiple transducers operating, the direction of the oscillation was ensured to be in-phase.

The Pressure Acoustic Module was applied to the fluid domain contained within the vessel walls. The material model was selected as viscoelastic fluid when modelling water.

### Meshing

The mesh was defined for each material individually as free tetrahedral mesh elements with maximum element size,  $h_{max} = \lambda/5$ , where  $\lambda$  refers to the wavelength of an acoustic wave for a given frequency for each material ( $c_s = f\lambda$ ). The mesh was both material and frequency dependent and therefore the model was re-meshed each time the frequency or structure (e.g. number of transducers) was changed.

### Extracting Results

To visualise the results 2D and 1D plots were plotted through the centre plane of the experimental rig. To do this a 2D XY plane was defined through the centre of the transducers as in Figure 3. From this 2D plane absolute acoustic pressure surfaces could easily be plotted. To compare the model results with experimental data taken from the rig 1D plots were used in COMSOL. This involved defining a 1D line along the Y axis of 2D XY plane shown in Figure 4.

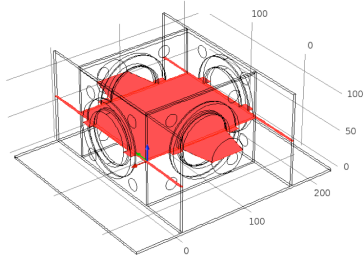


Figure 3. The XY plane used for extracting results from COMSOL simulations.

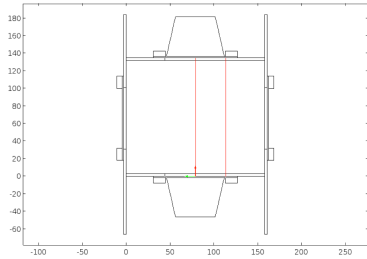


Figure 4. Measurement lines in red of the hydrophone through a plane at 62 mm above the base of the experimental rig and the lines used for extracting the 1D data from COMSOL.

### 3. Model Validation

#### Obtaining the Experimental Data

The validation of the model was performed using water as the fluid. This allowed the model to be solved and compared to experimental data taken from the rig. The experimental rig was filled with deionised water to a level of 120 mm. A Brüel Kjør 8103 hydrophone was used to measure the acoustic pressure at points in the water. The measuring point of the hydrophone was at 9 mm from the tip. The transducers were driven using an Aligent 33220A 20 MHz signal generator. A Tektronix DPO 2014B oscilloscope was used to monitor the output power of the signal generator and the voltage measured by the hydrophone. The measured voltage from the hydrophone was converted to a pressure through the following relationship from the hydrophone calibration specification:  $\mu V/Pa = 26.7$ .

Approximately 55 data points were taken through the centre of the fluid and halfway between the centre and the vessel wall at a hydrophone tip height of 53 mm from the base of the experimental rig (such that the acoustic centre of the hydrophone was at the vertical centre of the transducer face).

#### Comparison of Experimental and Model Results

Two variables were defined for the comparison of the model with the experiment: the oscillation frequency and the number of operating transducers. Three frequencies were used: 25.3 kHz,

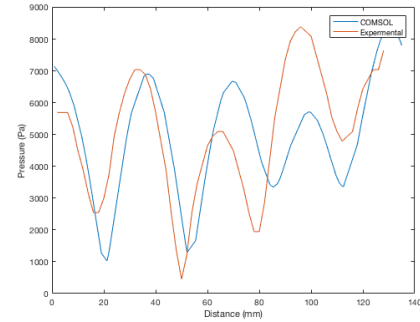


Figure 5. Comparison of the COMSOL results in blue with the experimental results in red for two transducers operating at 25.3 kHz in the reference medium (water).

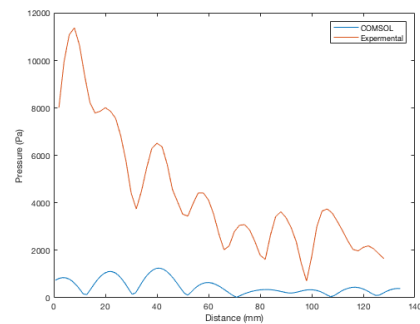


Figure 6. Comparison of the COMSOL results in blue with the experimental results in red for one transducer operating at 48.2 kHz in the reference medium (water).

48.2 kHz and 73.2 kHz which all corresponded to a low electrical impedance for the transducer(s) in use. Either one or two opposing transducers were activated allowing the model to be constrained to a symmetrical version reducing computation time.

Figure 5 shows the COMSOL model and experimental results plotted through the centre of the XY plane for two transducers emitting at 25.3 kHz. This plot shows a good agreement in both amplitude and transmitted frequency of the signal in the medium because the approximate power of the transducer was known for this frequency. Figure 6 shows the COMSOL model and experimental results plotted through the centre of the XY plane for a single transducer emitting at 48.2 kHz. The operating transducer is on the left of the plot. There is agreement between the pressure nodes and antinodes at 48.2 kHz but the amplitude of the peaks does not match because the power of the transducer was not previously known at this frequency.

#### Parameter Estimation

For the parameter estimation step of the model, the COMSOL Optimization Module was used. Within this module a least squares point objective was defined to match the experimental data obtained

from the experimental rig with the pressure at corresponding points within the model. A Nelder-Mead optimisation algorithm was selected due to its suitability for least squares fitting problems. The optimisation variable selected was the transducer power,  $P_{Trans}$ . Since the potential transducer power spanned several orders of magnitude (0.001 – 100 W) an exponent,  $n_{power}$ , was defined such that:

$$P_{Trans} = 10^{n_{power}}, \\ -3 \leq n_{power} \leq 2$$

The actual power transmitted to the transducer oscillation was dependent on the electrical impedance of the transducer and how well it was matched with the amplifier, which is frequency dependent. As such,  $P_{Trans}$  needed to be estimated for each frequency used. The values of  $P_{Trans}$  for each frequency are presented in Table 1.

Table 1. Transducer power values for each frequency from the parameter estimation study.

Frequency (kHz)	P trans (W)
25.3	0.6042
48.2	0.2376
73.2	0.6031

#### 4. Porous Material Model

The model was developed to study the interaction of acoustic fields with a metastable, reacting polymeric foam. The fully reacted, cured polymeric foam is a rigid polyurethane foam whose chemistry was formulated for this specific application to have large pores. The foam is as per the method shown in [8], and water was used to catalyze the reaction. The polymerisation reaction between the polyol and isocyanate runs in parallel to the expansion reaction of the isocyanate and water.

##### Elastic Waves

To model the propagation of the acoustic fields in the polymeric foam, the Poroelastic Waves interface was used. This interface solved Biot's equations for the coupled propagation of elastic waves in the elastic porous matrix and acoustic pressure waves in the saturating fluid.

The elastic wave equation can be obtained from Newton's second law:

$$\mathbf{F} = \rho \frac{\partial^2}{\partial t^2} \mathbf{u} - \nabla \cdot (\boldsymbol{\sigma}(\mathbf{u}) - s_0)$$

where  $\rho$  is the density,  $\mathbf{u}$  is the displacement vector,  $\boldsymbol{\sigma}$  is the Cauchy stress tensor, and  $s_0$  and  $\mathbf{F}$  represent

source terms. For the time-harmonic case in which displacement varies with time as  $\mathbf{u}(x, t) = \mathbf{u}(x)e^{i\omega t}$ , the equation for linear elastic waves reduces to the inhomogeneous Helmholtz equation:

$$\mathbf{F} = -\rho\omega^2\mathbf{u} - \nabla \cdot (\boldsymbol{\sigma}(\mathbf{u}) - s_0)$$

Biot developed the equations of linear elasticity for porous materials saturated with fluids [10]–[12]. In these equations the porous matrix is described through linear elasticity and the damping of waves is evaluated through the viscosity of the fluid. The theory uses bulk moduli and compressibilities of the matrix and fluid, which are independent of frequency. Again assuming time-harmonic displacements, Biot's equations for poroelastic waves are:

$$-\rho_{av}\omega^2\mathbf{u} + \rho_f\omega^2\mathbf{U} - \nabla \cdot \boldsymbol{\sigma} = 0 \\ -\rho_f\omega^2\mathbf{u} + \omega^2\rho_c(\omega)\mathbf{U} + \nabla p_f = 0$$

where  $\mathbf{u}$  and  $\mathbf{U}$  are the displacement vectors of the porous material and fluid respectively,  $\boldsymbol{\sigma}$  is the total stress tensor (fluid and porous material),  $p_f$  is the fluid pore pressure,  $\rho_{av}$  is the average density of the porous material, such that  $\rho_{av} = \rho_a + \varepsilon\rho_f$ , where  $\rho_a$  is the drained porous matrix density,  $\rho_f$  is the saturating fluid density and  $\varepsilon$  is the porosity, and  $\rho_c(\omega)$  is the complex density:

$$\rho_c(\omega) = \frac{\tau}{\varepsilon}\rho_f + \frac{\mu_f}{i\omega\kappa}$$

where  $\tau$  is the tortuosity,  $\mu_f$  is the fluid dynamic viscosity and  $\kappa$  is the permeability.  $\rho_c(\omega)$  represents the viscous drag on the fluid as a result of the pore structure.

##### Implementing the Poroelastic Material

The Poroelastic Waves interface was used to define an isotropic poroelastic material model. The metastable polymeric material was defined using Young's modulus and Poisson's ratio, measured from experiments. Biot's high frequency range limit was chosen since  $f \gg f_r$ , where the characteristic frequency  $f_r$ :

$$f_r = \frac{\mu_f}{2\pi a^2 \rho_f}$$

where  $a$  is the characteristic pore size. In the high frequency range, the dynamic fluid viscosity becomes frequency dependent,  $\mu_c(f)$ .

The Biot-Willis coefficient,  $\alpha_B$ , is estimated as 1 for the cured foam, since [13]:

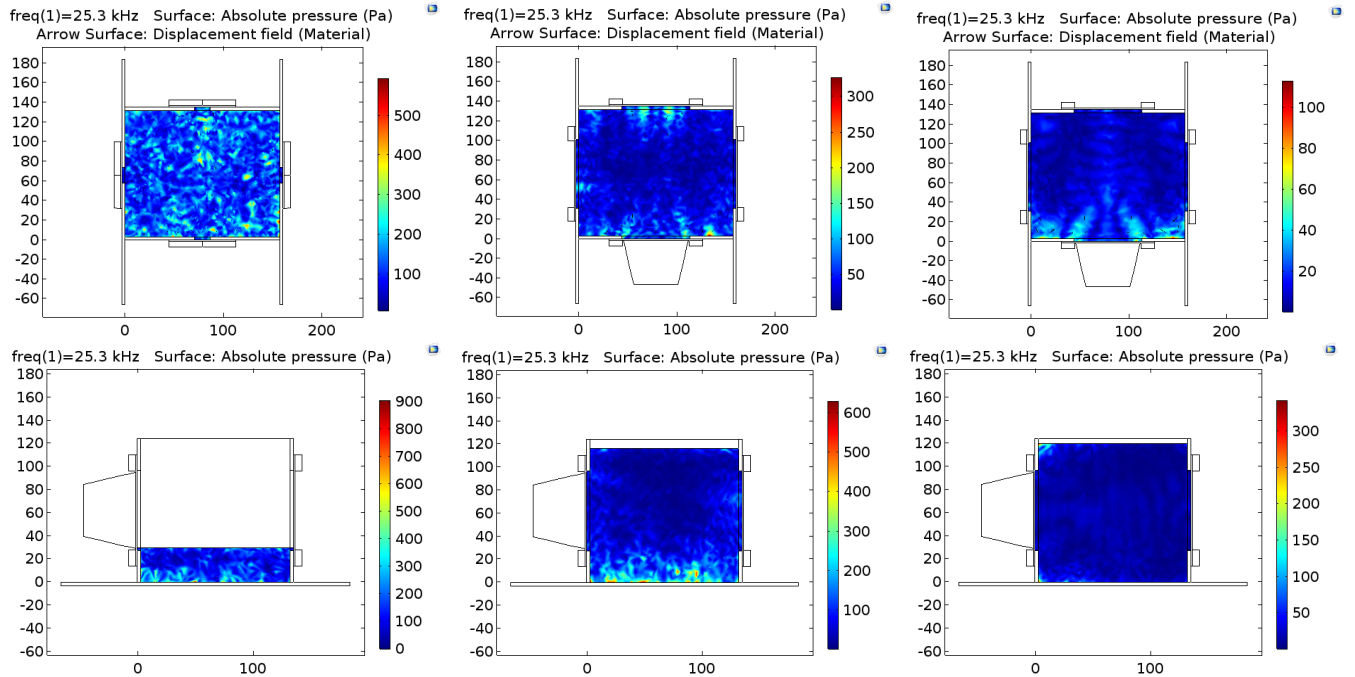


Figure 7. One transducer oscillating at 25.3 kHz, 100 W. From left to right, nucleation, rising and cured. The top row is an XY plane acoustic pressure (Pa) with the solid material velocity field displayed as arrows. The bottom row is the YZ plane acoustic pressure.

$$\alpha_B = 1 - \frac{\chi_s}{\chi}$$

where  $\chi_s$  is the compressibility of the solid and  $\chi$  is the compressibility of the porous material.

#### Parameters Used for the Polymeric Material

Three foam stages were considered for the model: (i) the *initial nucleation stage* where the bubble population was being created upon the addition of catalyst; (ii) the *viscoelastic foam stage* where the maximum height was reached but the polymerization reaction has not yet completed; and (iii) the *cured stage* where the final structure is formed and the polymerisation reaction is complete forming a rigid foam. The parameters for the model are detailed in Table 2. The values for the matrix material were measured from laboratory experiments or obtained from calculations. The fluid model was set to the properties of air.

Table 2. Values for parameters at different foaming stages: nucleation (Nuc.); viscoelastic (Visc.); and Cured.

Parameter	Nuc.	Visc.	Cured
Time of cure (minutes)	7	26	60
Volume of foam (% of cure)	25	97	100
Young's modulus of strut (Pa)	4.09E9	4.09E9	4.09E9
Drained Young's modulus (Pa)	1.63E7	2.29E6	1.19E7
Drained Poisson's ratio	0.375	0.375	0.375
Density of strut material (kg m <sup>-3</sup> )	1040	1040	1040
Drained density (kg m <sup>-3</sup> )	663.3	108.0	99.1
Porosity	0.36	0.89	0.90
Flow resistivity (N s m <sup>-4</sup> )	3750	3750	3750
Biot-Willis coefficient	1	1	1
Tortuosity	2.5	2.5	2.5
Fluid density (kg m <sup>-3</sup> )	1.2	1.2	1.2
Fluid dynamic viscosity (Pa s)	1.81E-5	1.81E-5	1.81E-5
Characteristic pore size (mm)	0.2	2	2

## 5. Results

The results of the simulations are presented for three frequencies (25.3 kHz, 28.2 kHz and 23.0 kHz) and three transducer configurations for each of the foam stages. Figure 7 shows the absolute pressure values of planes within the model for a single transducer oscillating at 25.3 kHz. Figure 8 shows the absolute pressure values of planes within the model for two transducers oscillating at 28.2 kHz. Figure 9 shows the absolute pressure values of planes within the model for four transducers oscillating at 23.0 kHz. In each figure the XY plane is plotted on the top row and the YZ plane is plotted on the bottom row, nucleation stage is the left, viscoelastic stage is the centre and cured stage is the right column. On the XY plane in the top row the material displacement vector is shown as a series of black arrows. The height of the XY plane is at the transducer centre for the viscoelastic (centre) and cured (right) plots. For the nucleation plot the XY plane is plotted 2 mm below the top surface of the porous medium (28 mm above the base of the experimental rig).

## 6. Discussion

In Figure 7, Figure 8 and Figure 9 a scattered pressure pattern can be seen during the nucleation stage. Nucleation sees the highest pressure values of all three foam stages but little material displacement. The random pattern is because only a small volume of the poroelastic material is in contact with the transducer, and thus the elastic waves diffract producing complex interference patterns.

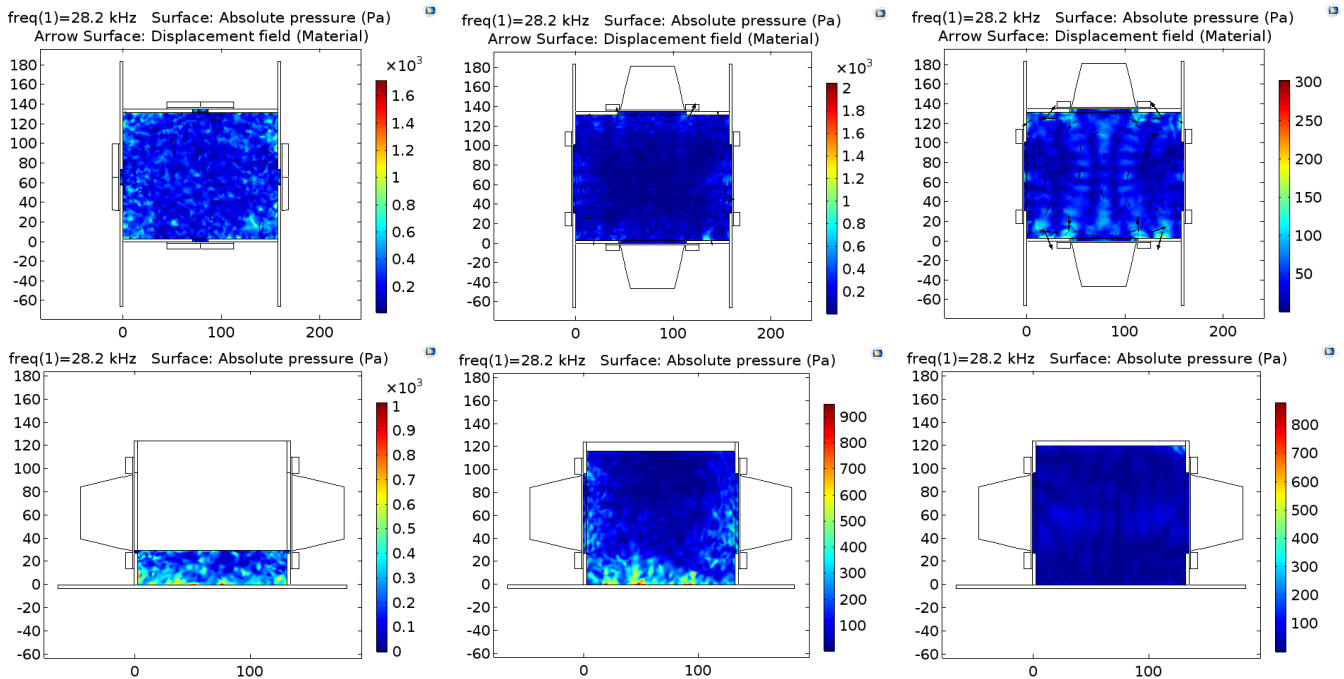


Figure 8. Two transducers oscillating at 28.2 kHz, 100 W each. From left to right, nucleation, rising and cured. The top row is an XY plane acoustic pressure (Pa) with the solid material velocity field displayed as arrows. The bottom row is the YZ plane acoustic pressure.

In the viscoelastic stage (central column) a more symmetrical pattern is formed in the XY planes with the majority of the pressure peaks residing at the edges of the rig. The pressure peaks in the YZ plane are held at the bottom of the poroelastic material domain, except for the four transducer case in Figure 9. The pressure values are typically less than the nucleation stage. This is likely to be the result of the lower material density and lower bulk modulus of the drained porous material. At this stage the polymeric material that makes up the struts of the foam is not yet solid and will not propagate elastic waves efficiently since the structure will tend to dampen the amplitude of the waves.

In the cured foam pressure plots (right column) the results are significantly more symmetrical. The pressure amplitudes are low but the material displacements are high, suggesting more efficient transmission of elastic waves through the solid porous matrix. The majority of the displacement can be seen around the edges of the experimental rig in Figure 8, however there is little displacement in Figure 7. This is because of the low-pressure amplitudes of Figure 7 since only a single transducer is transmitting into the poroelastic material. The high pressure and displacement regions of Figure 9 are mostly in the centre of the porous material.

### Implications for the Manufacture of FGM

A bubble of a size less than resonance will travel up a pressure gradient towards the pressure antinodes [9]. When this concept is applied to a large population of bubbles it is expected that smaller bubbles will convene on pressure antinodes, whilst larger bubbles will head towards the pressure nodes. A control of where the pressure nodes and antinodes are is therefore required to control the resulting

porous structure of the polymeric foam. Results such as those in the cured stage of Figure 9, where there is a large region of high pressure in the centre of the porous material, would be exciting to replicate in the lab in the hope of producing samples with a functional density gradient. If the acoustic field can be adequately controlled then the density gradients could be designed for specific load cases.

The results from this simulation show that there are significant changes in the pressure fields due to the evolution of the poroelastic material at the different stages of the polymerisation of the foam. As such, a better understanding of the properties of the material throughout the stages is required. It has been shown in previous works that the rising and packing stages of foaming are most sensitive to acoustic radiation [14], [15]. An improved material model to represent these stages is required to study how the pressure field will evolve during these stages.

## 7. Conclusions

This paper has presented a validated model to simulate the effect of ultrasonic transducers on a fluid based on an experimental rig design. A poroelastic material model was then developed to represent a metastable polymeric material at three different stages of the polymerisation reaction. High pressures dominate the initial nucleation stage with a scattered distribution throughout the material. Once the strut material of the porous structure becomes viscoelastic (i.e. rising stage) the pressure patterns become more symmetrical with lower pressure amplitudes. Finally, once the polymer cures the pressure patterns become similar to those previously seen in water (the reference medium) with a symmetric shape and clear nodes and anti-nodes. To apply this

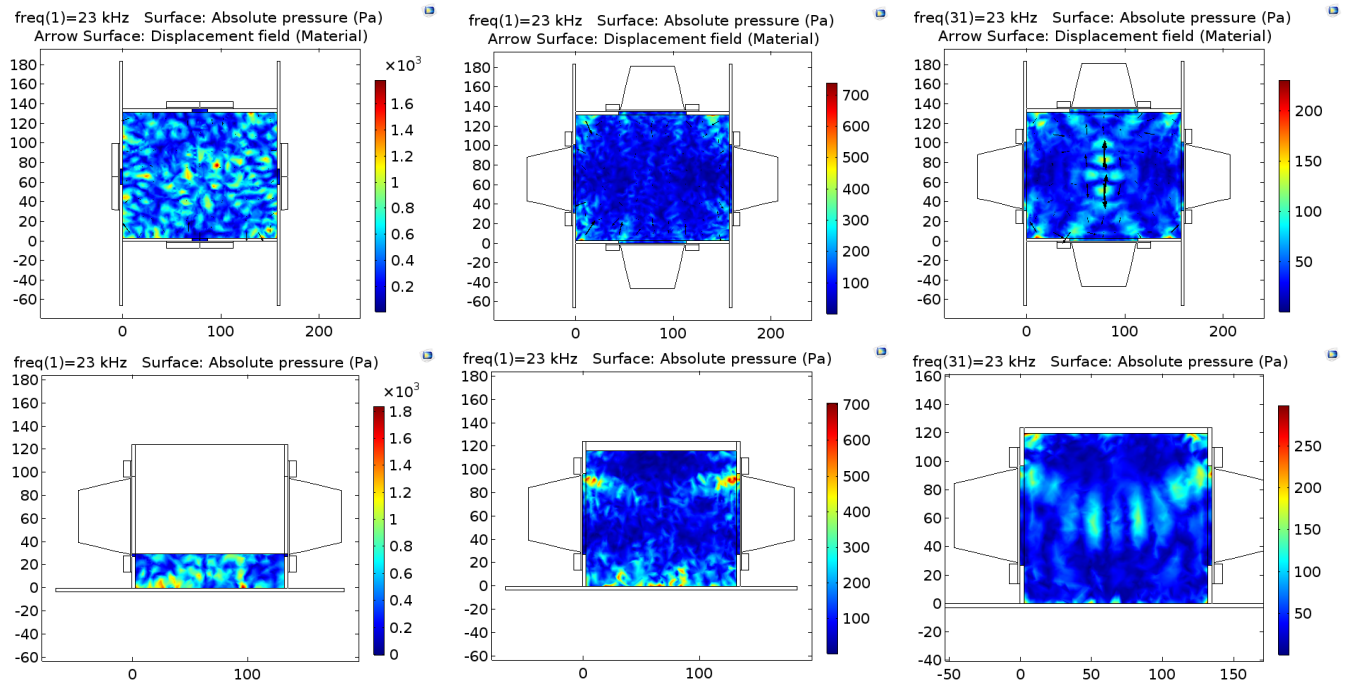


Figure 9. Four transducers oscillating at 23.0 kHz, 100 W each. From left to right, nucleation, rising and cured. The top row is an XY plane acoustic pressure (Pa) with the solid material velocity field displayed as arrows. The bottom row is the YZ plane acoustic pressure.

computational model to the manufacture of control porosity gradients in graded materials an improved material model is needed.

## 8. Future Work

The future work for this project will entail developing a more accurate material model in the Poroelastic Waves interface. Then comparing the simulated results to physical samples produced through experimentation to try to correlate the pressure seen in the poroelastic model to the resulting porosity distribution within the cured polymeric foam.

## 9. References

- [1] A. Neubrand, *Functionally Graded Materials*. 2001.
- [2] S. S. Wang, "Fracture mechanics for delamination problems in composite materials," *J. Compos. Mater.*, vol. 17, no. 3, pp. 210–223, 1983.
- [3] S. Ruiyi, G. Liangjin, and F. Zijie, "Truss Topology Optimization Using Genetic Algorithm with Individual Identification Technique," *Proc. World Congr. Eng. 2009 Vol II*, vol. II, 2009.
- [4] J. a Sethian and a Wiegmann, "Structural Boundary Design via Level Set and Immersed Interface Methods," *J. Comput. Phys.*, vol. 163, no. 2, pp. 489–528, 2000.
- [5] Y. M. Xiet and G. P. Steven, "A Simple Approach To Structural Optimization," *Comput. Struct.*, vol. 49, no. 5, pp. 855–896, 1993.
- [6] B. Kieback, A. Neubrand, and H. Riedel, "Processing techniques for functionally graded materials," *Mater. Sci. Eng. A*, vol. 362, no. 1–2, pp. 81–105, 2003.
- [7] M. Naebe and K. Shirvanimoghaddam, "Functionally graded materials: A review of

fabrication and properties," *Appl. Mater. Today*, vol. 5, pp. 223–245, 2016.

- [8] J. R. Corney and C. Torres-Sanchez, "Towards functionally graded cellular microstructures," *Jorunal Mech. Des.*, vol. 131, pp. 1–8, 2008.
- [9] T. G. Leighton, *The Acoustic Bubble*. London: Academic Press Ltd, 1994.
- [10] M. A. Biot, "Theory of Propagation of Elastic Waves in a Fluid-Saturated Porous Solid. II. Higher Frequency Range," *J. Acoust. Soc. Am.*, vol. 28, no. 2, pp. 179–191, 1956.
- [11] M. A. Biot, "Theory of Propagation of Elastic Waves in a Fluid-Saturated Porous Solid. I. Low-Frequency Range," *J. Acoust. Soc. Am.*, vol. 28, no. 2, pp. 168–178, 1956.
- [12] J.F.Allard and N. Atalla, *Propagation of Sound in Porous Media*. 2009.
- [13] M. A. Biot and D. G. Willis, "The elastic coefficients of the theory of consolidation," *J. Appl. Mech.*, vol. 24, pp. 594–601, 1957.
- [14] C. Torres-Sanchez and J. Corney, "Identification of formation stages in a polymeric foam customised by sonication via electrical resistivity measurements," *J. Polym. Res.*, 2009.
- [15] C. Torres-Sanchez and J. Corney, "Porosity tailoring mechanisms in sonicated polymeric foams," *Smart Mater. Struct.*, vol. 18, 2009.

## 10. Acknowledgements

Thanks go to the EPSRC funded Centre for Doctoral Training in Embedded Intelligence (CDT-EI) and Far-UK Ltd. for sponsoring this research. Additional thanks go to the collaborator German Garcia-Romero.